

Co-registration of White Matter Tractographies by Adaptive-Mean-Shift and Gaussian Mixture Modeling

Orly Zvitalia, Arnaldo Mayer*, Ran Shadmi, Shmuel Miron, and Hayit Greenspan

Abstract—In this paper we present a robust approach to the registration of white matter tractographies extracted from DT-MRI scans. The fibers are projected into a high dimensional feature space based on the sequence of their 3D coordinates. Adaptive mean-shift (AMS) clustering is applied to extract a compact set of representative fiber-modes (FM). Each FM is assigned to a multivariate Gaussian distribution according to its population thereby leading to a Gaussian Mixture model (GMM) representation for the entire set of fibers. The registration between two fiber sets is treated as the alignment of two GMMs and is performed by maximizing their correlation ratio. A 9 parameters affine transform is recovered and eventually refined to a 12 parameters affine transform using an innovative mean-shift (MS) based registration refinement scheme presented in this paper. The validation of the algorithm on synthetic intra-subject data demonstrates its robustness to interrupted and deviating fiber artifacts as well as outliers. Using real intra-subject data, a comparison is conducted to other intensity based and fiber-based registration algorithms, demonstrating competitive results. An option for tracking-in-time, on specific white matter fiber tracts, is also demonstrated on the real data.

Index Terms—Brain,DTI,Tractography,Registration.

I. INTRODUCTION

THIS During the last decade, Diffusion Tensor-Magnetic Resonance Imaging (DT-MRI) has been successful in providing a quantitative description of water molecules random diffusion motion in the brain white matter [1], [2]. In particular, the orientation information as modeled by the diffusion tensors has opened the way to in-vivo reconstruction of white matter fiber tracts, for which many tractography algorithms, both deterministic [3], [4], [5], [6] and probabilistic [7], [8], have been developed. As with structural MRI, registration is an important issue for tractography data. Intra-subject registration of fiber tracts can be useful for longitudinal studies aimed at therapy efficacy evaluation or disease progression assessment [9], [10]. Inter-subject registration is an important tool for tract based population studies [11], and tract modeling or atlas

construction [12], [13].

In previous works, three main alternative approaches were considered for the registration of tractography data: scalar or vectorial registration, tensor registration and fiber registration. In *scalar or vectorial registration*, the registration is computed based on one or more channels of scalar images extracted from the DT-MRI images [14], [15], [16]. One advantage of performing registration based on scalar images is that classical scalar (intensity based) registration methods can be used. However, these methods do not take into account the directional information entailed in the tensors. Therefore, tensors are to be re-oriented during or after the registration in order to preserve fiber tracts coherence. In [14], a very high dimensional elastic registration procedure termed "Hierarchical Attribute Matching Mechanism for Elastic Registration" (HAMMER) is used to recover the spatial transformation by co-registering T_1 weighted images. Once the transformation is recovered, it is applied to the diffusion tensors. In another work, a multiple-channels demons algorithm [17] has been proposed to compute a non-linear deformation field between voxels [15]. Several combinations of channels are considered and investigated. A different approach that incorporates the diffusion weighted images in a multi-channel registration scheme is [16], in which affine co-registration is performed according to the corresponding acquisition gradient directions using mutual information (MI) as a similarity measure.

In *tensor registration*, the registration of DT-MRI images is performed directly between the tensor fields. In this case, the tensorial values are taken into account simultaneously during registration, thereby better enforcing local orientation information than with scalar registration. Computational cost, however, is usually higher than with scalar methods. This approach has attracted most of the research focus in the field of DT-MRI registration. In [18] a multi-channel deformable registration based on the demons algorithm is proposed. Registration is performed using T_2 weighted images and transformation invariant tensor characteristics (i.e., three tensor eigenvalues). By using transformation invariant tensor features, the computationally expensive step of tensor reorientation is avoided. The sum of squared differences is used for tensor similarity measurement. Alternatively, a method based on highly structured points identification has been used for local matching of DT data [19]. A Multi-channel non-rigid registration based on directional information of the tensor is proposed in [20]. The similarity measure used is the multivariate mutual information (MI) calculated from the tensor components and T_2 weighted

Manuscript received January 19, 2009; revised July 14, 2009.

Asterisk indicates corresponding author.

O. Zvitalia, *A.Mayer, R. Shadmi and H. Greenspan are with the Department of Biomedical Engineering, Tel-Aviv University, Ramat-Aviv 69978, Israel (e-mail: arnmayer@gmail.com).

S. miron is with the Multiple Sclerosis Center, Sheba Hospital, Tel-Hashomer, Israel (e-mail:Shmuel.Miron@sheba.health.gov.il).

Color versions of one or more of the figures in this paper are available online at <http://ieeexplore.ieee.org>.

Copyright (c) 2009 IEEE. Personal use of this material is permitted. However, permission to use this material for any other purposes must be obtained from the IEEE by sending a request to pubs-permissions@ieee.org.

images. MI has also been used as similarity measure in [21] for non-rigid DTI registration based on a viscous fluid model. In this work, it is assumed that MI can implicitly handle the nonlinear intervoxel intensity differences, eliminating the need for tensor re-orientation during the optimization procedure. A Piecewise affine registration in a multi-resolution framework has also been proposed for tensor registration [22]. It is based on a tensor distance defined using the L^2 inner product of diffusion profiles. This similarity measure is used to optimize the tensor reorientation explicitly. Two different approaches, both direct and feature based, have been proposed by [23] for DTI registration. The direct approach defines the diffusion tensor constancy constraint (DTCC), an extension of the well known brightness constancy constraint used for scalar images optical flow. The feature based method is based on the spectral properties of the rotation group and requires point correspondences in the image. In [24], an affine registration algorithm is proposed, based on a point-wise tensor similarity measure which is based on the overlap between tensor modes. Directional and magnitude information are weighted differently depending on the type of diffusion. A few of these tensor based metrics were evaluated and compared in [25].

Most recently, a third approach was proposed in which registration is performed directly at the tractographic fibers level [26], [27], [28], [29], [30]. We term this approach the *Fiber registration* approach. Here, the directional information entailed in the diffusion tensors is naturally inherited by the reconstructed WM fiber tracts and further enhanced by the connectivity information described by each fiber trajectory. In [26], curvature and torsion features have been used to describe each fiber in a multi-scale framework. A mean squared difference is then used to measure similarity between fibers at different scale levels. Most similar fibers are matched and used to fit a global rigid transform. The method is based on rotation and translation invariance of the curvature and torsion features, therefore it is limited to rigid registration. Moreover, since matching is performed between individual fibers, this method is computationally expensive. It is demonstrated for an intra-subject registration scenario. In another work, the fibers are represented by their spatial coordinates sequences and considered as points in a high dimensional feature space [27]. Affine registration is then resolved by an efficient iterative closest feature point algorithm (called ICF) that tackles the computational bottleneck of high dimensional search by implementing approximate nearest neighbors techniques. The method is applied to inter-subject registration and the construction of a probabilistic map of the Corticospinal tract is demonstrated. In [28], bundle-based nonlinear registration is proposed. First, linear registration based on fractional anisotropy (FA) scalar images is performed between the set of brains to be aligned and an atlas template in order to enable automated atlas based segmentation of major bundles. Correspondence between these major bundles is also obtained across the brains. Next, using the set of bundle based correspondences, a smooth and invertible poly-affine transform is calculated and applied to the data.

In the current work, we address the affine registration of intra-subject brain tractographies and its application to the tracking in time of specific WM tracts. The proposed method belongs to the fiber-based registration category. The fibers are projected into a high dimensional feature space defined by the sequence of their 3D coordinates. Adaptive mean-shift (AMS) clustering is applied to extract a compact set of representative fiber-modes (FM). Each FM is assigned to a distinct multivariate Gaussian distribution. Assigning each of the Gaussians with a weight proportional to its fiber population leads to a Gaussian Mixture Model (GMM) representation for the entire set of fibers. The registration between two fiber sets is treated as the alignment of two GMMs and is performed by maximizing their correlation ratio. A 9 parameters affine transform is recovered and eventually refined to a 12 parameters affine transform using an innovative mean-shift (MS) based registration refinement scheme. In this work we extend and validate the registration method proposed in [29], [30]. The main contributions of the current work are:

- The proposed method does not require any initial alignment between the corresponding MRI or DTI scans.
- The FM sets are equivalent to landmarks used in point based registration, which in our case are extracted automatically. Moreover, the number of the representative FMs is an output of the algorithm and not a user preset parameter.
- A continuous registration framework is provided for a 9 parameter affine registration between the FM sets.
- The registration is extended to fully affine using a novel mean-shift based refinement procedure.
- The method robustness is demonstrated for major tractography artifacts: split fibers, deviating fibers and outliers.
- The method is compared with two state-of-the-art registration methods, one intensity based and one fiber-based, for real intra-subject data.
- Intra-subject tracking in time of WM tracts is demonstrated on real pathologic data, enabling detection of selected tracts in follow-up brain scans.

The remainder of this paper is organized as follows. The proposed method is detailed in section II. Experimental results are provided in section III and discussed in section IV.

II. METHODS

The proposed algorithm consists of five main steps, as presented (in rectangles) in Figure 1. The *preprocessing* step includes removal of fibers which are too short, re-sampling of fibers to a fixed length fiber descriptor, and orientation standardization. Following preprocessing, *Adaptive-Mean-Shift* (AMS) clustering is applied to the model and target fiber sets in order to extract a compact and reliable set of representative fibers for each, hereon termed the fiber modes (FM) set. Each FM set is next assigned to a distinct multivariate Gaussian distribution. The resulting set of Gaussians, each of them weighted proportionally to its fiber population, leads to a GMM representation. The registration between two fiber sets is treated next as the alignment of two GMMs, and is performed by maximizing their correlation ratio. A 9 parameter affine

transformation is recovered and eventually refined to a 12 parameter affine transformation using an innovative mean-shift (MS) based registration refinement scheme. Each step is described in detail in the following subsections.

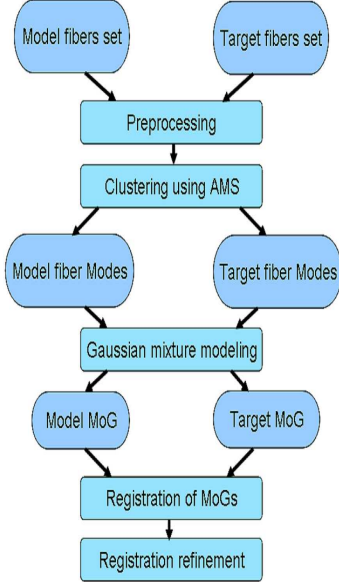


Fig. 1. Flowchart of fiber-based registration algorithm

A. Preprocessing

Tractography softwares produce fiber descriptors using sequences of their 3D coordinates. The number of point samples along each fiber and the spacing between consecutive points depends on the fiber's length and shape. The preprocessing phase in the current work consists of the following set of operations. First, fibers shorter than 10mm are removed since most of them correspond to artifacts located outside the brain. In order to achieve a constant length fiber descriptor, each fiber is re-sampled at $P = 20$ equally spaced points resulting in a $d = 3P = 60$ -dimensional feature vector generated by concatenating the samples' (x,y,z) coordinates. The number of sampling points is an empirical compromise between dimensionality and fidelity to the original representation (see section III-A2 for details). Each fiber can be represented by two flipped (forward and backwards) point sequences. This may cause two spatially adjacent fibers to be considered distant. In order to standardize fiber descriptors, we calculate the signed differences vector between each fiber's ending points, that is, $\Delta = \{x_P - x_1, y_P - y_1, z_P - z_1\}$. A fiber descriptor is flipped when the largest amplitude component of its Δ vector is negative. By doing so, we impose that each fiber be represented by a sequence of increasing coordinate values along its major variation axis. For example, if the coordinates origin is located in the bottom-left-rear corner, vertical fibers will run bottom-to-top, lateral fibers will run left-to-right and longitudinal fibers rear-to-front.

B. Clustering using Adaptive Mean-shift

The amount of fibers describing a full WM tractography is very large. It is necessary to find a compact and reliable set of representative fibers in order to reduce the computational complexity of the algorithm. In this work, a set of representative fibers is extracted by clustering each of the fiber sets to be registered, using the AMS [31] algorithm. The clustering procedure produces a set of fiber clusters each represented by a representative fiber, hereafter termed fiber-mode (FM). The FMs are equivalent to landmarks used in point based registration, which in our case are extracted automatically by clustering.

The AMS is an iterative procedure which estimates the local maxima, or modes, of the underlying density distribution for a given data set, in a selected feature space [31]. The underlying assumption in this procedure is that regions of high density in the feature space correspond to local maxima of the original probability density function of the data [32]. It is important to note that the number of modes is an output of the mean shift algorithm and is not pre-set by the user. This is particularly useful for tractography data for which the number of fiber clusters may be difficult to set a-priori. Furthermore, the number of modes is usually much smaller than the original number of data points and hence the amount of data to be registered is significantly reduced.

Consider n vectors in a d -dimensional feature space $\mathbf{x}_i \in \mathbb{R}^d$. As defined in subsection II-A, we have $d=3P=60$. To derive the mean-shift (MS) we begin by defining the *sample point* estimator at location \mathbf{x} :

$$\hat{f}_K(\mathbf{x}) = \frac{1}{n} \sum_{i=1}^n \frac{1}{h_i^d} k\left(\left\|\frac{\mathbf{x} - x_i}{h_i}\right\|^2\right) \quad (1)$$

where \mathbf{k} is the profile of the kernel \mathbf{K} such that

$$\mathbf{K}(x) = c_{d,k} k(\|x\|^2) > 0 \quad \|x\| \leq 1 \quad (2)$$

and $c_{d,k}$ is a normalization factor used to ensure $\mathbf{K}(x)$ integrates to 1.

h_i is the bandwidth assigned to the kernel for data point x_i . It is defined per data point x_i as follows [33]:

$$h_i = \|\mathbf{x}_i - \mathbf{x}_{i,k}\|_1 > 0 \quad (3)$$

where $\mathbf{x}_{i,k}$ is the k th nearest neighbor of vector \mathbf{x}_i .

Provided that the derivative of the profile \mathbf{k} exists, the function $g(x)$ can be defined:

$$g(x) = -k'(x). \quad (4)$$

Another kernel $\mathbf{G}(x)$ can be defined using $g(x)$ as a profile:

$$\mathbf{G}(x) = c_{d,g} g(\|x\|^2) \quad (5)$$

Taking the gradient of equation (1), the following expression for the mean-shift vector can be obtained:

$$\mathbf{m}_G(x) = C \frac{\hat{\nabla} f_K(x)}{\hat{f}_G(x)} = \frac{\sum_{i=1}^n \frac{x_i}{h_i^{d+2}} g\left(\left\|\frac{x-x_i}{h_i}\right\|^2\right)}{\sum_{i=1}^n \frac{1}{h_i^{d+2}} g\left(\left\|\frac{x-x_i}{h_i}\right\|^2\right)} - x \quad (6)$$

Equation (6) shows that the mean shift vector is proportional to the normalized gradient of density estimate, as computed

from kernel K . Thus, the mean shift vector points at the direction of maximum density increase [34]. Moreover, since the magnitude of the mean shift vector depends on the inverse of the density estimation using kernel G , it gradually decreases as we move closer to locations of high density. Data points lying in regions of high density will be assigned with smaller kernel bandwidths h_i and affect narrower neighborhood, but since these points are weighted by $1/h_i^{d+2}$ they are given high importance. Conversely, points lying in low density areas are assigned with larger kernel bandwidths but have lower importance as their weights are smaller [33].

The *mean-shift* procedure is recursively defined by evaluating the mean shift vector, $m_G(x)$, and moving along it. Starting from a point y_0 in the feature space, we have:

$$y_{j+1} = \frac{\sum_{i=1}^n \frac{1}{h_i^{d+2}} x_i g\left(\left\|\frac{y_j - x_i}{h_i}\right\|^2\right)}{\sum_{i=1}^n \frac{1}{h_i^{d+2}} g\left(\left\|\frac{y_j - x_i}{h_i}\right\|^2\right)} \quad (7)$$

Each point used in the initialization step moves towards a spot of local maximum density independently [35]. This procedure was proven to converge to a stationary point (i.e., point of zero gradient) in the underlying density estimation function resulting in a mode candidate [33]. The result of this iterative procedure is a series of points each located in an area of higher density than the previous one, until convergence. In the following we will refer to each convergence point as a FM. In order to extract all the FMs for a given brain tractography, equation (7) is computed iteratively for every fiber descriptor until convergence. Fibers that converge into the same FM are naturally associated to the same cluster. The detected FMs are cluster centers and the shapes of the clusters are determined by their basins of attraction [32]. It is important to note that neighborhood queries computed in equation (7) constitute a real bottleneck for the mean-shift algorithm. This is especially true for large data-sets in high dimensional spaces, where a naïve computation of all the neighborhood queries at each mean-shift iteration becomes prohibitive. Recently, [31] adapted an approximate method for computing the neighborhood queries to high dimensional computer vision data. The method is based on the locality sensitive hashing (LSH) technique [36]. In LSH, feature vectors are placed into a hash table structure where neighbor points lie in the same bucket of the hash table with a high probability. The described LSH framework was recently extended to L_p norms [36]. LSH structure allows to retrieve neighborhoods with high efficiency in comparison with the naïve approach since only a small number of points are now tested by equation (7) at each mean-shift iteration. This is called the fast adaptive mean-shift (FAMS) algorithm [37] and is the basis of the proposed fiber clustering algorithm.

1) Using Mean-Shift modes as landmarks for registration:

In the proposed algorithm, registration is based on the two FM sets obtained by clustering. These FM sets provide a reliable representation (or landmarks) of the entire data set, within the selected feature space. In order to perform registration accurately, invariance of the FM sets to spatial transformations is required. Ideally, for intra subject registration, one FM set is expected to be the exact transformation of the other FM set. Formally, denote \mathbf{x} and \mathbf{y} , two $3P$ -dimensional fiber sets

related by a spatial transformation, such that

$$\mathbf{y} = \mathbf{T}\mathbf{x}. \quad (8)$$

where \mathbf{T} is a $3P \times 3P$ transformation matrix. Also denote two sequences of the mean locations x_j and y_j (equation (7)) initialized using two corresponding points namely, $y_0 = \mathbf{T}x_0$, belonging to \mathbf{y} and \mathbf{x} , respectively. It can be easily shown (see Appendix) that the AMS-fiber modes are invariant under spatial transformations which consist of translation, rotation and uniform scaling. Namely,

$$m_y = m_x + t \quad ; \quad m_y = Rm_x \quad ; \quad m_y = \alpha m_x \quad (9)$$

where t is a translation vector, R is an orthogonal rotation matrix and α is a uniform scaling factor.

However, in the case of anisotropic scaling, the relative positions between sample points are not preserved making the influence of the spatial transformation of the FM sets hard to predict as it depends on the transformation parameters and the initial spatial distribution of the samples points in the feature space.

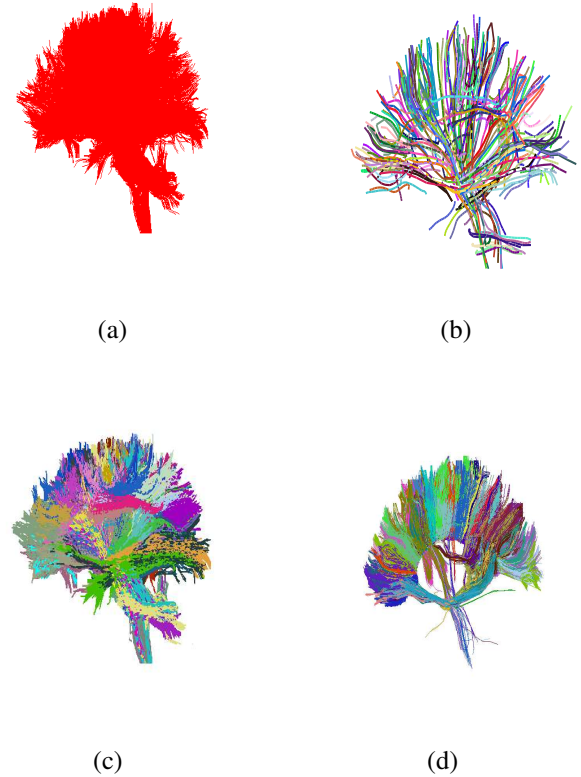


Fig. 2. Results of AMS clustering: (a) The original set (approximately 100000 fibers); (b) clustering into 261 FMs by the AMS; (c) the clustered fibers; (d) The corpus callosum represented by 88 modes and their corresponding fibers.

Figure 2 illustrates the results of applying the AMS clustering on a set of fibers representing a full WM tractography.

Figure 2(a) shows the entire fiber set which consists of approximately 100000 fibers. Figure 2(b) shows 261 fiber modes obtained by applying the AMS algorithm to the full fiber set, each FM is colored by a unique color. Figure 2(c) shows the 261 clusters represented by these FMs, each cluster's fiber population bears the color of its mode. In order to illustrate the correspondence between clusters and anatomical tracts, 88 specific clusters representing the corpus callosum were extracted as shown in Figure 2(d).

C. Gaussian mixture modeling

Following clustering, we obtain two sets of fiber modes. Each FM represents a population of fibers which is of a particular size and spatial distribution. In the following, we will treat registration as the alignment of two mixtures of Gaussians (GMMs) [38]. For this purpose, we model each FM set by a GMM. Each Gaussian corresponds to a distinct FM and is defined in a 3P-dimensional feature space, by the following parameters: a *mean vector*, a *scalar weight*, and a *covariance matrix*, defined as follows: The *mean* is a $3P \times 1$ feature vector of the corresponding FM. The *weight* is the ratio between the number of fibers assigned to the FM and the total number of fibers. The *covariance matrix* is defined to be $\lambda \mathbf{I}$ where \mathbf{I} is the identity matrix of size $3P \times 3P$ and λ is a scalar constant. For each Gaussian, λ is defined to be the average variance of all the elements in all the fibers belonging to the current FM. The resulting model and target GMMs have M_n and T_n components, respectively. The parameter P can be set by the user. As was previously mentioned, in the clustering phase fibers are represented using $P = 20$. This representation results in high computational cost in the registration process. A coarser representation may be used in the GMMs registration step in order to enable sufficiently accurate results while maintaining a reasonable computational cost. Therefore, we chose to use $P = 1$ for the GMM registration step of all the registration experiments (i.e., each fiber mode is represented by its center point). For the AMS clustering, we keep $P = 20$ since the preservation of the fiber shape information is important to obtain similar clusters for the model and the target.

D. Registration of GMMs

The basic idea of the proposed registration method is to measure the correlation between two fiber sets by considering their continuous approximations [38]. Formally, consider two GMMs, f and g of size M_n and T_n , respectively (Φ denotes a normal distribution):

$$f(x) = \sum_{i=1}^{M_n} \alpha_i \Phi(x|\mu_i, \Sigma_i) \quad (10)$$

$$g(x) = \sum_{i=1}^{T_n} \beta_i \Phi(x|\nu_i, \Gamma_i) \quad (11)$$

$$\Phi(x|\mu, \Sigma) = \frac{1}{(2\pi)^{d/2} |\Sigma|^{1/2}} \exp\left(-\frac{1}{2}(x - \mu) \times \Sigma^{-1}(x - \mu)^T\right) \quad (12)$$

The 9 parameters affine transformation relating these GMMs can be parameterized by a non-singular block diagonal $3P \times 3P$ matrix \mathbf{A} , and a translation vector \mathbf{t} of size $3P \times 1$. Each block element along the diagonal of \mathbf{A} is the basic affine transformation matrix of size 3×3 built out of the rotation and scaling parameters. \mathbf{t} is simply the concatenation of the translation parameters t_x, t_y, t_z repetitively. For the purpose of reorientation of covariance matrices, \mathbf{A} is factorized using a polar decomposition $\mathbf{A} = \mathbf{Q}\mathbf{S}$ resulting in an orthogonal and symmetric rotation matrix \mathbf{Q} and a symmetric matrix \mathbf{S} . Only the rotation matrix is applied to the covariance matrix. The correlation between two GMMs is given by the expression:

$$\sigma_{fg} = \int fg dx = \sum_{i=1}^{M_n} \sum_{j=1}^{T_n} \alpha_i \beta_j \int \Phi(x|\mu_i, \Sigma_i) \Phi(x|\nu_j, \Gamma_j) dx. \quad (13)$$

Transforming f using the above mentioned transformation we get:

$$f_{A,t}(x) = \sum_{i=1}^{M_n} \alpha_i \Phi(x|A\mu_i + t, Q\Sigma_i Q^T) \quad (14)$$

We find the optimal transformation between these GMMs by maximizing the following correlation ratio:

$$E = \frac{\sigma_{fg}^2}{\sigma_f^2 \sigma_g^2}. \quad (15)$$

Using the formula

$$\int \Phi(x|\mu, \Sigma) \Phi(x|\nu, \Gamma) dx = \Phi(0|\mu - \nu, \Sigma + \Gamma) \quad (16)$$

The cost function used for maximization can be written explicitly:

$$E = \frac{N_E}{D_E} \quad (17)$$

Where

$$N_E = \left(\sum_{i=1}^{M_n} \sum_{j=1}^{T_n} \alpha_i \beta_j \Phi(0|A\mu_i + t - \nu_j, Q\Sigma_i Q^T + \Gamma_j) \right)^2 \quad (18)$$

And

$$D_E = \sum_{i=1}^{M_n} \sum_{j=1}^{M_n} \alpha_i \alpha_j \Phi(0|A(\mu_i - \mu_j), Q(\Sigma_i + \Sigma_j) Q^T) \times \sum_{i=1}^{T_n} \sum_{j=1}^{T_n} \beta_i \beta_j \Phi(0|\nu_i - \nu_j, \Gamma_i + \Gamma_j) \quad (19)$$

Since the cost function being maximized is differentiable, gradient based optimization methods can be used for solving it. In this work we used the *fmincon* function from the MATLAB optimization toolbox to optimize the correlation ratio between the model and target GMMs.

E. Refinement of the registration

Intra-subject registration of real data requires the handling of anisotropic scaling between the fiber sets as well as various amounts of noise. The FMs representing each fiber set may therefore be slightly different. For this reason, a refinement procedure is suggested next in order to improve registration results. In the proposed refinement phase, the full FM descriptors are used (i.e., each FM is again represented by a 60×1 feature vector) in order to account for local fiber shape information. Refinement is achieved as follows:

- 1) Apply the 9 parameter transformation recovered by GMM registration to the model FMs.
- 2) Embed the warped model FMs into the full target fibers population.
- 3) Run the AMS procedure from each warped model FM according to equation (7).

In this case x_i are the full target fiber set and y_0 are the warped model FMs. Assuming the warped model FMs lie within the basin of attraction of their corresponding target FMs, by the end of the AMS iterations, each warped model FM will converge into its corresponding target FM.

In Figure 3 we illustrate the registration process at different steps of the algorithm. The target brain tractography was synthetically created by applying an affine transform to the model brain tractography. Red fibers are model modes and blue fibers are target modes. The misaligned FM sets are shown in Figure 3(a). The FM sets after GMMs registration are shown in Figure 3(b). The FM sets following registration refinement are shown in Figure 3(c). The overlap between the FM sets can be seen to increase as the algorithm progresses. Following the registration refinement procedure, pairs of model-target FMs are used to establish correspondences between the non-warped model FMs and the target FMs. A 12 parameters affine transformation is established using the robust Random Sample Consensus (RANSAC) scheme [39] on the set of corresponding coordinates. The 12 parameters affine transformation fitting procedure was implemented as follows:

- 1) Given a set of non-warped-model and target correspondences, randomly choose a subset of a predefined size S and find the 12 parameters using Least-Squares.
- 2) Apply the recovered transformation on the entire non-warped model FMs and calculate the error.
- 3) Repeat 1-2 until a predefined number of trials Nt .
- 4) Find the set of parameters resulting in the minimum error. The error for each set of parameters is defined to be the sum of the absolute differences between the warped model FMs (according to the transformation recovered from the current subset of correspondences) and target FMs. The values of two parameters, S and Nt , are chosen according to the following considerations: 12 parameters are to be estimated. A single fiber descriptor is therefore sufficient as it provides 20 point correspondences. However, as previously explained, anisotropic scaling and noise may cause corresponding modes to be somewhat different. Therefore, a transformation recovered from a single pair of corresponding modes may be inaccurate. It is recommended to use more correspondences for the transformation estimation. The chosen value for S

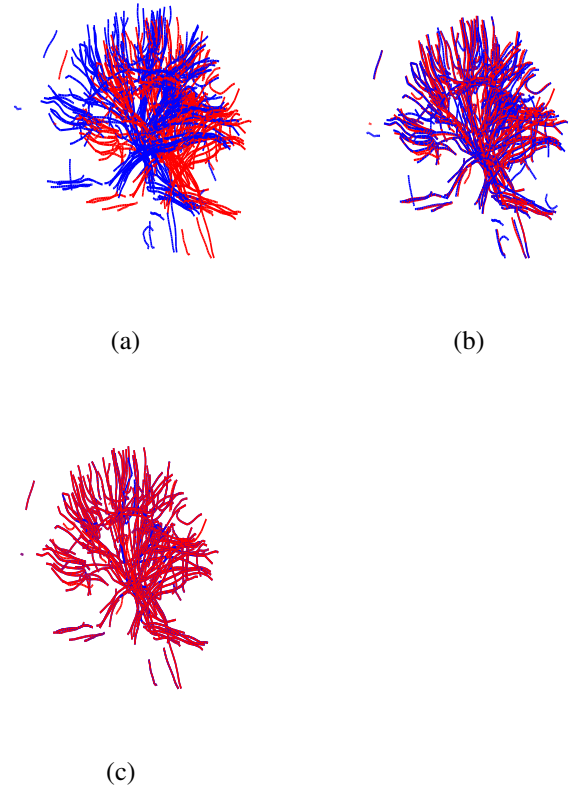


Fig. 3. Model (red) and Target (blue) modes at different steps of the registration algorithm. (a) misaligned FM sets; (b) FM sets after GMMs registration; (c) FM sets following registration refinement.

is a compromise between computational cost and robustness to correspondences inaccuracies. The number of trials Nt chosen should be large enough to provide sufficient outliers elimination. Assuming there are C correspondences available, the total number of combinations of choosing S out of C is $C!/S!(C-S)!$. Theoretically, an exhaustive search of all possible combinations will provide the optimal set of parameters. However, such a search is computationally intractable and hence the number of trials should be much smaller than the total number of possible combinations.

III. EXPERIMENTS AND RESULTS

In this section the proposed method is validated using synthetic registration experiments on real brain datasets. The method is also demonstrated in a real registration scenario in which two time points from an MS patient brain data are analyzed. We first provide a sensitivity analysis of the AMS-GMM fiber-based algorithm. Then, using the AMS-GMM fiber-based registration, we compare results to several other registration methodologies and demonstrate intra-subject tracking in time of WM tracts.

A. Synthetic registration experiments

1) *Data Set*: The data used in the synthetic experiments is real DTI data downloaded from Johns Hopkins University

medical (JHU) MRI lab¹. Tractographies were obtained using DTIstudio [40]. Intra-subject data was simulated by applying predefined 12 parameters affine transformations on a set of tractographies. The original and transformed fiber sets are denoted as the model and target sets being registered, respectively. FM sets were extracted by applying AMS clustering separately to the model and target sets. The bandwidth for each sample point was determined by considering its 200 nearest neighbors ($k_n = 200$). In the refinement procedure, the number of available correspondences C is approximately 250, the subset size of correspondences S was set to 30 and the number of trials Nt was set as 500. Note that the total number of possible combinations is approximately 10^{38} . Hence, the number of trials chosen is much smaller as desired.

2) *Fiber representation validation*: The tractography software provides non uniform length fiber descriptors. These fiber descriptors are re-sampled at equally spaced points along fibers to create uniform length fiber descriptors. The standardized fiber descriptor is an approximation of the originally reconstructed fiber as illustrated in Figure 4.

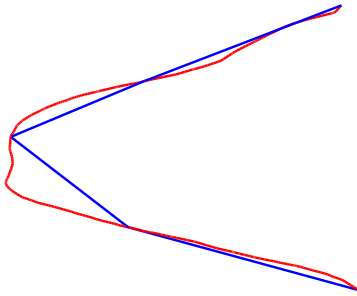


Fig. 4. Approximated fiber as a result of re-sampling. The red fiber is the original full fiber descriptor. The blue fiber is the approximated fiber using $P=5$ sample points.

Fidelity of the re-sampled fiber to the original fiber must be preserved. One fidelity preserving solution is to up-sample all fibers according to the longest fiber descriptor in the fiber set. However, using such descriptors directly increases computational cost, and is probably not necessary since a coarser representation may preserve the fiber's shape. The number of sample points per fiber is thus a compromise between two considerations: fidelity to the original fiber's shape and computational complexity.

The following experiment was done in order to determine the optimal number of samples needed per fiber. Full brain tractographies² with an average of 45 ± 44 points per fiber descriptor were taken into account. The following steps were taken:

- All fiber descriptors of a full brain were up-sampled to create a uniform length representation of 350 points each.

¹<http://lbam.med.jhmi.edu/>.

²Brain No. 2 from the JHU data set

This representation will hereon be referred to as the *full fiber descriptor*.

- Fibers shorter than 22mm were ignored since approximation errors are most likely to occur in long fibers where the uniform spacing step is relatively large.
- Each of the remaining fibers was then re-sampled at varying numbers of equally spaced sample points and the error between the full fiber descriptor and the approximated fiber was measured. The error was defined based on the distance between each point in the full fiber descriptor to the approximated fiber. The approximation error for each fiber was defined as the maximum distance between a point in the full fiber and the approximated fiber. The overall error per brain, was obtained by averaging the approximation error for all fibers (approximately 54000 fibers).

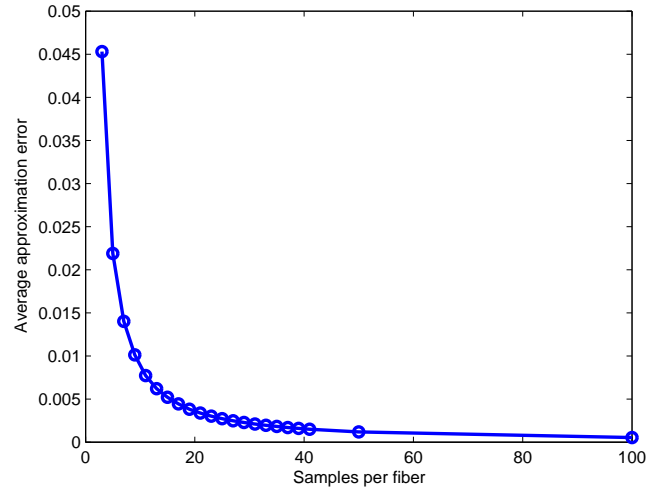


Fig. 5. Average approximation error as a function of the number of samples per fiber.

Results are presented in Figure 5. As expected, the average approximation error decreases as the number of samples per fiber increases. For a small number of sample points the approximation error is large. With increased numbers of sample points the gain in error reduction diminishes. The knee of the error plot is around 15 samples per fiber. In the presented experiments, we select to use 20 samples per fiber.

3) *Robustness tests*: Fiber-based registration methods rely on tractography results. Therefore, they are naturally exposed to common tractography artifacts such as interrupted (split) or deviating fiber tracts. Fiber splitting and deviation can occur when the fractional anisotropy (FA) along a fiber decreases (due to noise) to a level that interferes with the fiber tracking. The tracking algorithm may terminate, resulting in an interrupted fiber, or the algorithm may proceed in the wrong direction, producing a deviated tract. Low FA values can also be a result of multiple fibers with different directions intersecting in the same voxel. In this case, the FA computed from the tensor model is of low value even though there are several dominant directions within the voxel. In addition

to data related problems, different decision criterions in line propagation tractography algorithms may be the cause for splitting or deviating fibers. The above-described artifacts may interfere with the registration process and hence robustness to them is required. Several robustness tests for the proposed registration algorithm were performed.

In the following experiments, the model consisted of the original fiber set and the target sets were obtained by adding noise artifacts (split or deviating fibers) or by dropping fibers to create outliers and applying the transformation to the resulting fiber set. AMS clustering was applied to the model and target sets separately. Initialization of the GMMs optimization procedure was conducted as follows: The centers of mass of both the model and the target FM sets were calculated and the difference between them was used to initialize translation parameters. No rotation or scaling was assumed in the initialization.

Registration accuracy is measured by computing the root mean squared error (RMSE) between the model and target full fiber sets, prior to registration and following it. The remaining error following registration, hereon termed the *residual RMSE*, is computed by the following ratio:

$$residualRMSE = \frac{RMSE_f}{RMSE_i} \times 100 \quad (20)$$

where $RMSE_i$ is the root mean squared error between originally misaligned fiber sets and $RMSE_f$ is the root mean squared error between the aligned fiber sets. In each of the following robustness experiments, two types of results are produced depending on the way the RMSE errors were averaged :

- over the entire JHU 15 brains data-set warped by a single synthetic affine transform.
- over 10 distinct affine transforms applied to a single JHU brain.

The corresponding results will be termed as *brain averaged* or *transform averaged* accordingly.

4) *Robustness to split fibers*: Split fibers were simulated by selecting a random set of fibers and splitting each selected fiber at an arbitrary point along its length. An interrupted fiber is illustrated in Figure 6(a). The entire curve is the original fiber. A small segment (shown in green) is cut out of the original fiber. This results in two shorter fibers that are created (shown in red and blue). The transformation parameters used in the *brain averaged* splitting artifacts experiment are: $\theta_x = -7^\circ$, $\theta_y = 5^\circ$, $\theta_z = 3^\circ$, $t_x = 5\text{mm}$, $t_y = 8\text{mm}$, $t_z = -6\text{mm}$, $s_x = 1.1$, $s_y = 0.95$, $s_z = 1$, $s_{xy} = -0.05$, $s_{xz} = 0.05$, $s_{yz} = -0.03$. Where θ_i are the rotation angles, t_i are the translation parameters, S_i are the scaling factors and S_{ij} the skews. For the *transform averaged* experiment, brain nr. 4 from JHU was selected. Ten distinct affine transforms were generated by randomly selecting the parameters within the ranges defined by Table I under certain magnitude constraints. For example, the rotations around the x and y axes (θ_x, θ_y) are randomly selected in the $[-10^\circ, -5^\circ] \cup [5^\circ, 10^\circ]$ interval while the rotation around z is randomly selected in the $[-20^\circ, -5^\circ] \cup [5^\circ, 20^\circ]$ interval (rows 2-4 of column 1 in Table I). Among the

randomly drawn combinations, only those that correspond to a rotation amplitude $\|\theta\| = \sqrt{\theta_x^2 + \theta_y^2 + \theta_z^2} \geq 15^\circ$ are kept. The same concept is applied to translation (second column, Table I), scaling (third column) and skew (last column) selection. The amplitude constraints are listed in the last row of Table I.

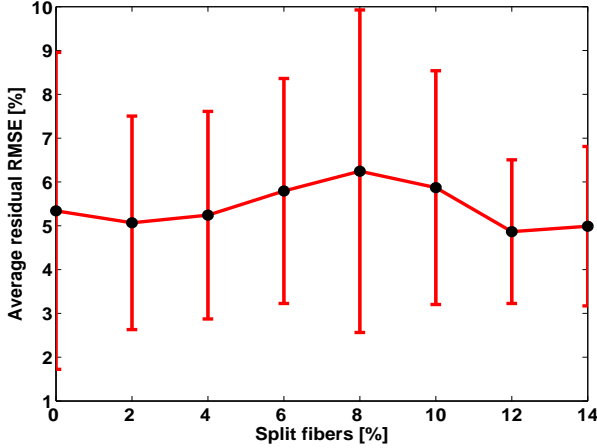
Residual error statistics for the splitting experiment are provided in Figures 7(a) and (b). In the *brain averaged* fiber splitting experiment (Figure 7(a)), the mean residual error is lower than 6.5% for up to 14% of split fibers. The *transform averaged* fiber splitting experiment (Figure 7(b)) produced even lower mean residual errors values, below 2.7%, for the same range of interrupted fibers amount. Hence, we observe robustness across a wide range of interrupted fiber amount.

5) *Robustness to deviating fibers*: Fiber deviations were simulated by randomly selecting a set of fibers, then splitting each fiber at an arbitrary point creating two tails and reconnecting one of the tails to the nearest fiber tail within the entire fiber set. Only fiber extremities closer than 10mm are considered for reconnection. In order to preserve fibers smoothness, tails may only be reconnected when the resulting fiber turning angle is smaller than 70 degrees. The fiber deviation artifact is illustrated in Figure 6(b). The original fiber, in red, was altered to create the deviated fiber, in blue. The transformation parameters used in the *brain averaged* deviating artifact experiment are: $\theta_x = 5^\circ$, $\theta_y = -7^\circ$, $\theta_z = 9^\circ$, $t_x = 5\text{mm}$, $t_y = -8\text{mm}$, $t_z = 4\text{mm}$, $s_x = 1.09$, $s_y = 0.85$, $s_z = 1$, $s_{xy} = 0.08$, $s_{xz} = -0.05$, $s_{yz} = -0.09$. For the *transform averaged* experiment, the same brain (JHU nr. 4) and transformation selection method is used as for the splitting experiment. Residual errors statistics for the deviated fibers experiment are provided in Figures 7(c) and (d). For the *brain averaged* deviated fibers experiment (Figure 7(c)), the mean residual errors are below 8% for up to 14% deviated fibers. The *transform averaged* deviated fibers experiment (Figure 7(d)) produced even lower mean residual errors values, below 2.7%, for the same range of interrupted fibers amount. Hence, robustness across a wide range of deviated fiber amount is also provided.

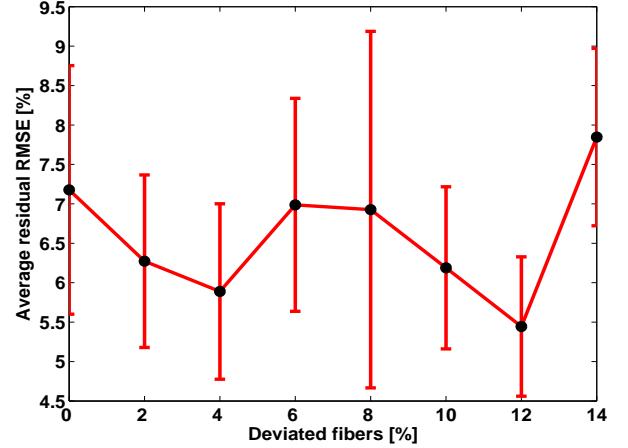
6) *Robustness to outliers*: Robustness of the algorithm to fiber outliers was examined next. In our context, an outlier fiber is a fiber with no correspondence in the other set. Different amounts of fibers from the model fiber set were randomly selected and dropped (removed) prior to registration. The amount of dropped fibers is the amount of outliers simulated. Registration was performed between the reduced model fiber set and the full target fiber set. The transformation parameters used in the *brain averaged* outliers experiment are: $\theta_x = 4^\circ$, $\theta_y = 8^\circ$, $\theta_z = 5^\circ$, $t_x = 13\text{mm}$, $t_y = -8\text{mm}$, $t_z = 5\text{mm}$, $s_x = 1$, $s_y = 0.95$, $s_z = 1.1$, $s_{xy} = 0.05$, $s_{xz} = -0.05$, $s_{yz} = 0.08$. For the *transform averaged* outliers experiment, the same brain (JHU nr. 4) and the same transformations selection method is used as for fiber splitting and deviating experiments. Figure 8 shows mean residual RMSE results for different amounts of outliers. The mean residual errors for the *brain averaged* experiment is below 4.5% for up to 20% outliers. For the

TABLE I
RANGES FOR THE RANDOM TRANSFORM PARAMETERS. THE LAST ROW GIVES THE MAGNITUDE CONSTRAINT FOR ROTATIONS, TRANSLATIONS, SCALINGS AND SKEWS.

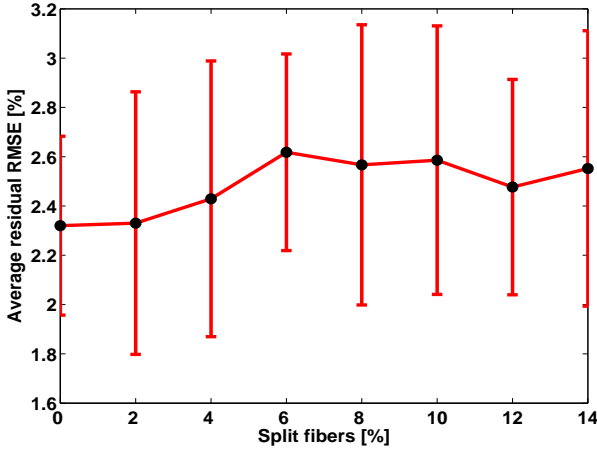
Rotation[°]		Translation[mm]		Scaling		Skew	
θ_x	$\pm(5 - 10)$	t_x	$\pm(13 - 26)$	S_x	$1 \pm (0.05 - 0.2)$	S_{xy}	$\pm(0.03 - 0.1)$
θ_y	$\pm(5 - 10)$	t_y	$\pm(13 - 26)$	S_y	$1 \pm (0.05 - 0.2)$	S_{xz}	$\pm(0.05 - 0.18)$
θ_z	$\pm(5 - 20)$	t_z	$\pm(15 - 30)$	S_z	$1 \pm (0.05 - 0.2)$	S_{yz}	$\pm(0.05 - 0.18)$
15°		35mm		0.15		0.18	



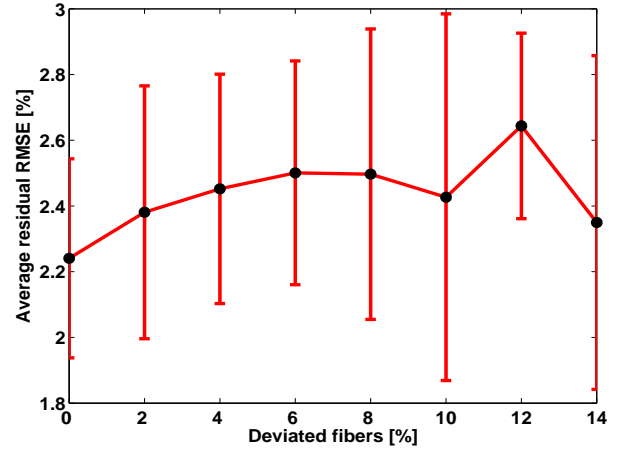
(a)



(c)



(b)



(d)

Fig. 7. Mean Residual RMSE results for different amounts of split fibers (a) averaged over 15 brains; (b) averaged over 10 affine transforms. Mean residual RMSE for different amounts of deviated fibers (c) averaged over 15 brains ; (d) averaged over 10 affine transforms.

transform averaged experiment, the mean residual error is below 2.4% for up to 20% outliers. Therefore, we observe robustness across a wide range of outlier amounts.

B. Real registration experiments

1) *Data Set*: The data used for real registration and tract tracking experiments consists of a pair of DWI acquisitions for the same subject. The data was provided by the multiple sclerosis center of Sheba Medical Center³. The time interval between the acquisitions (time points) is 10 months. The subject is a 34 years old male that was diagnosed with relapsing-remitting multiple sclerosis. The disease duration is 10 years.

Both acquisitions were made on the same 3T GE Signa MRI machine. Each of them included 31 gradient weighted volumes and two reference volumes (B0) with a voxel size of $1 \times 1 \times 2.6mm^3$ and 56 axial slices. Diffusion tensors and tractography were computed using DtiStudio as previously done for the synthetic experiments data. Figure 9 shows 3 sample T2 weighted slices for the considered brain acquired at the first time point. In these slices, lesions clearly appear as hyper-intense stains on the white matter (a few sample lesions are circled in white). Full brain tractographies at the first and second time points generated approximately 78000 and 81000 fibers, respectively. This difference in fiber quantity requires robustness to outliers, a property that was demonstrated in the synthetic data experiments in subsection III-A6.

³The Multiple Sclerosis Center , Sheba Hospital, Ramat-Gan, Israel.

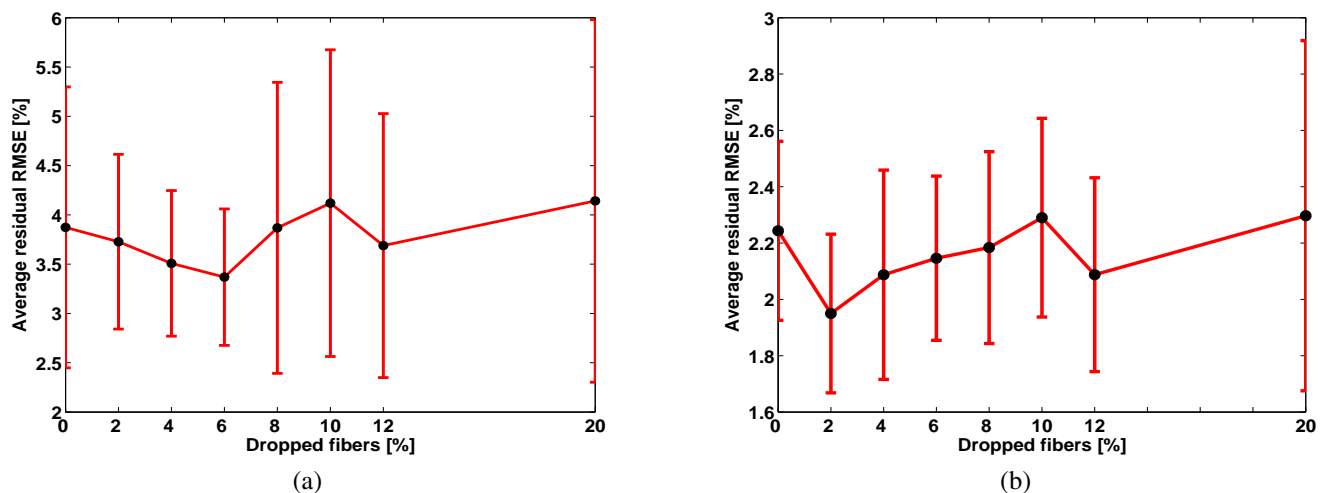


Fig. 8. Mean Residual RMSE results for different amounts of outliers (a) averaged over 15 brains; (b) averaged over 10 affine transforms.

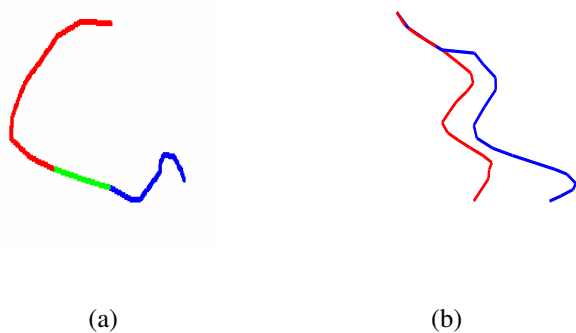


Fig. 6. (a) Interrupted fiber. The full curve is the original fiber, the green segment is cut and two fibers are created instead (red and blue segments) which are shorter than the original fiber; (b) Deviating fiber. Red curve is the original fiber, blue curve is the resulting fiber due to deviation.

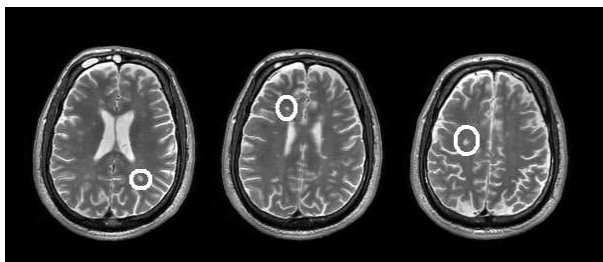


Fig. 9. Three sample T2 weighted slices for the considered brain acquired at the first time point. In these slices, lesions clearly appear as hyper-intense stains on the white matter. A few lesion samples are circled in white.

2) *Comparison to other methods:* In the following experiment, the affine registration accuracy of the proposed method, hereon termed AMS-GMM, is compared to the state-of-the-art intensity based method, FLIRT [41]. FLIRT is the affine registration tool of the well known FSL software package [42]. The algorithm is based on a multi-start, multi-resolution global optimization method. It was applied to the data using the

default parameters values for the recovery of a 12 parameters affine transform as advised by the authors. Comparison is also provided with the fiber-based registration algorithm ICF [27]. ICF performs direct registration of tractographic fibers through an efficient high-dimensional extension of the iterative closest point algorithm [43]. ICF was also applied to recover a 12 parameters affine transform using the parameters recommended by the authors⁴.

Our goal is to perform accurate registration of tractographies. Therefore, the fiber-level residual RMSE measurement defined in previous experiments is still appropriate.

Each of the compared methods (AMS-GMM, FLIRT and ICF) recovers a distinct affine transform that is consecutively applied to warp the model fibers. In this experiment model and target fibers belong to distinct DTI acquisitions. Correspondence between model and target fibers is not known a-priori as was the case in the synthetic registration scenario. Prior to the RMSE computation, an additional required step is to retrieve the nearest target fiber for each warped model fiber in order to create corresponding fiber pairs. Nearest fibers are efficiently recovered using the LSH framework under L_2 norm as described in II-B. Table II gives the obtained residual RMSE for the AMS-GMM, FLIRT and ICF registrations. For our method, two different values of k_n (the number of neighbors considered for bandwidth computation before AMS) are considered. We can see that for both k_n values the residual RMSE for our method is very similar to the other methods RMSE. In particular, for $k_n = 100$, our RMSE is about 2.4% better than for FSL or ICF. Lower k_n values result in a larger number of modes that possibly better represent the fiber set. Figures 10 and 11 are sagittal and coronal views, respectively, for time point 1 (green) fibers in overlap with time point 2 (blue) fibers (a) before registration and (b) after registration by AMS-GMM, (c) by ICF, and (d) by FSL. The registration results for AMS-GMM correspond to $k_n=100$. From the figures, we conclude that good and similar visual

⁴ICF parameters values: Down-sampling ratio for the model set (D_s) = 1/50, number of ICF iterations (l_{itn}) = 12, number of RANSAC iterations (R_{it}) = 500.

results are obtained for the three compared methods.

TABLE II
RESIDUAL RMSE FOR THE PROPOSED METHOD (AMS-GMM), FLIRT,
AND ICF REGISTRATIONS.

Method	parameters	res.RMSE
AMS – GMM	$k_n = 200$	0.6084
AMS – GMM	$k_n = 100$	0.5886
FLIRT	default	0.6034
ICF	$D_s = 1/50, I_{tn} = 12, Rit = 500$	0.6047

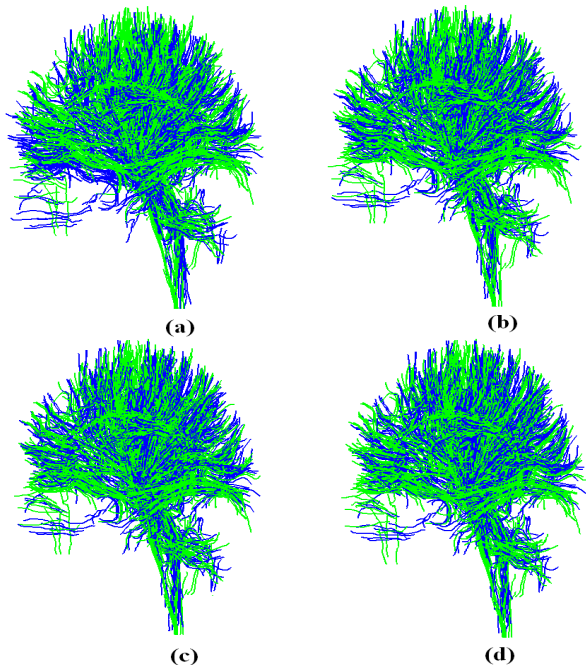


Fig. 10. Sagittal view for time point 1 fibers (green) in overlap with time point 2 fibers (blue). (a) Before registration; (b) After registration by AMS-GMM; (c) After registration by ICF; (d) After registration by FSL .

3) *Intra-subject tracking in time of WM tracts*: In this experiment we demonstrate the ability of our method to track tracts-of-interest (TOI) manually segmented from the first acquisition (model brain) into the second acquisition (target brain). This is, to our knowledge, the first attempt to automatically track in time WM tracts in real intra-subject data. For this purpose, the same pathologic brain is used as in the previous experiment. The first step is to perform AMS clustering starting from each TOI fiber in the full model population in order to extract the model TOI FMs. Direct registration between the TOI FMs and the full target brain FMs increases the risk of converging into a local minima. This results from the fact that simple-shaped TOIs may happen to be represented by a small number of FMs that contains poor shape characteristics. The corticospinal is an example of simple-shaped TOI consisting of near straight-line shaped fibers (red in Figure 13). In case of a significant initial misalignment, its FMs may erroneously be matched to non-related linearly shaped WM structures that correspond to local

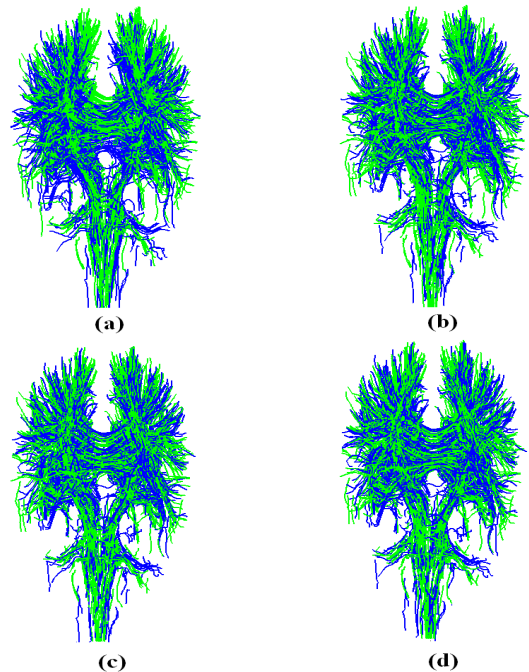


Fig. 11. Coronal view for time point 1 fibers (green) in overlap with time point 2 fibers (blue). (a) Before registration; (b) After registration by AMS-GMM; (c) After registration by ICF; (d) After registration by FSL .

minima of the GMM registration cost function. In order to avoid this problem, the TOI FMs are padded with a certain amount of randomly selected FMs from the model brain. The padding enhances the shape information content of the original TOI. A constant padding amount of 40% (of the total number of model FMs) is used for all the following TOI experiments. Registration is then performed between the padded model FMs and the full target FMs using our method. Eventually, the recovered transform is applied to the model fibers and the corresponding target fibers are extracted by returning for each warped model fiber, the nearest target fiber. Here again, nearest fibers are efficiently recovered using the LSH framework under L_2 norm described in II-B. Results for the Corpus Callosum, the Corticospinal (left and right) and Uncinate (left) tracts are shown in Figures 12, 13 and 14 respectively. The first column (a) shows the manual segmentation of the TOI fibers (red) in overlay with the model brain FMs (blue). The second column (b) shows the automatic segmentation of the tracked TOI fibers (red) at the second acquisition in overlay with the target brain FMs (blue). Top rows are sagittal views, bottom rows are coronal views.

IV. DISCUSSION

In this work a novel method for direct registration between WM tractographies was presented. This method does not require registration between tensor images or other MRI scans. Registration at the fiber level strongly enforces 3D shape and connectivity consistency. For example, different points along one fiber cannot be assigned with points of two different fibers during the registration process. These constraints are

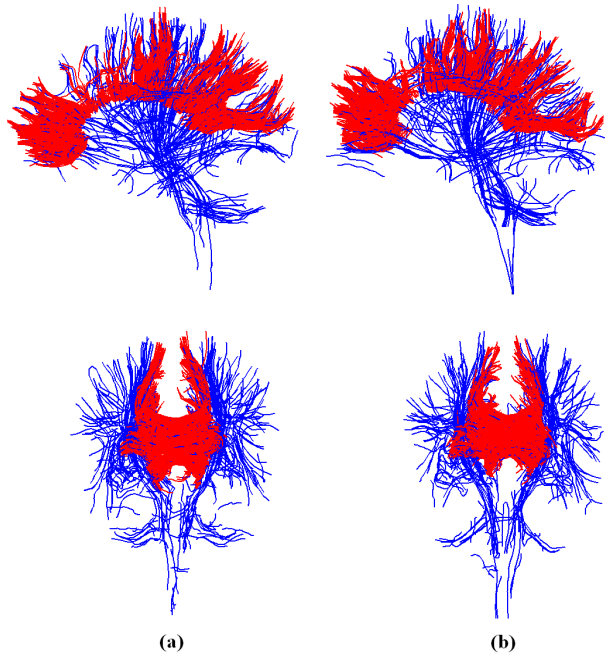


Fig. 12. Results for the Corpus Callosum: the first column (a) shows the manual segmentation of the TOI fibers (red) in overlay with the model brain FMs (blue). The second column (b) shows the automatic segmentation of the tracked TOI fibers (red) at the second acquisition in overlay with the target brain FMs (blue). Top rows are sagittal views, bottom rows are coronal views.

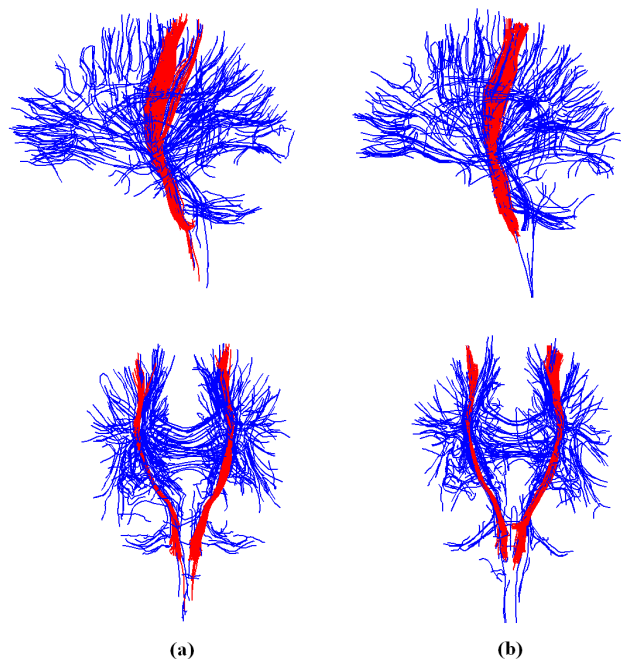


Fig. 13. Results for the Corticospinal (left and right): the first column (a) shows the manual segmentation of the TOI fibers (red) in overlay with the model brain FMs (blue). The second column (b) shows the automatic segmentation of the tracked TOI fibers (red) at the second acquisition in overlay with the target brain FMs (blue). Top rows are sagittal views, bottom rows are coronal views.

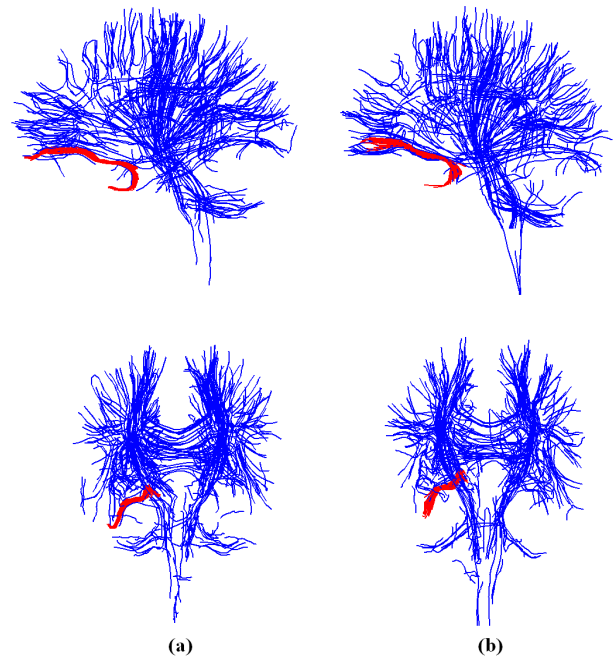


Fig. 14. Results for the Uncinate (left): the first column (a) shows the manual segmentation of the TOI fibers (red) in overlay with the model brain FMs (blue). The second column (b) shows the automatic segmentation of the tracked TOI fibers (red) at the second acquisition in overlay with the target brain FMs (blue). Top rows are sagittal views, bottom rows are coronal views.

difficult to formalize and maintain using point or tensor based registration methods.

A compact set of representative fibers, termed fiber modes, is extracted by AMS clustering in order to reduce the amount of data considered for registration. The fiber modes are equivalent to automatically extracted landmarks and are more informative than randomly selected fibers. AMS clustering is initiated from each data point in the feature space. The resulting number of modes and their respective position is therefore an output of the clustering procedure with no need for initialization. This is particularly useful as the number of fiber clusters reliably representing a full WM tractography is difficult to set a-priori. Another strong point of the AMS is the ability to process large datasets as encountered with full WM tractography, typically containing more than 100,000 fibers. In comparison, spectral clustering based methods [28] are limited by the maximal practical size of the similarity matrix.

Following clustering, fiber clusters are modeled by continuous GMMs according to each mode's population, and global registration is achieved by maximizing the correlation ratio between the two GMMs using a gradient based optimization algorithm. Experimental results show that the coarse representation in the GMMs registration phase is sufficient for performing accurate registration. This is the case since the Gaussians parameters originate in the highly detailed 60 dimensional representation used for clustering.

The AMS based refinement procedure improves registration by handling local variations in modes position due to spatial transformations and noise. Experimental results show that

AMS procedures that are initiated from each of the warped model modes eventually converge into the corresponding target modes. This indicates that the transformation recovered by the GMMs registration phase was sufficiently close to the real transformation, or in other words, the warped model modes lie within the basins of attraction of their corresponding target modes.

The proposed method demonstrated robustness to large amounts of missing fibers (fiber outliers) and tractography artifacts (splitting and deviating fibers) on the Johns Hopkins University DTI data set for synthetic registration experiments. Validation on a real registration scenario was also presented for a pathologic brain (multiple sclerosis) scanned at two different time points. In this task, the presented method compared favorably with two other registration methods: the intensity based FLIRT and the fiber-based ICF. Due to the current scarce availability of real intra-subject DTI data, it is not yet possible to conclude if the proposed method outperforms the intensity based methods on a statistical basis. Serial DTI acquisitions have been quite recently introduced for patient follow-up in WM diseases. Moreover, the consecutive acquisitions are usually separated by several month periods, thereby delaying the availability of acquisition pairs for the same subject. We believe, however, that depending on the registration purpose one of the methods may be more appropriate. For example, if the final purpose is to align scalar FA images to perform voxel based statistics, the use of an intensity based method is more intuitive as it seeks the optimization of a cost function that explicitly depends on voxels/tensors values correspondence. On the contrary, if the final goal of registration is to extract corresponding WM tracts in different brains, the use of a fiber-based method is more intuitive as it seeks the optimization of a cost function that explicitly depends on fibers positions correspondence. Automatic time-tracking capability was also successfully demonstrated on the same data for the corpus callosum, Corticospinal and Uncinate tracts. This is, to our knowledge, the first attempt to automatically track in time WM tracts in real intra-subject data.

Several directions are currently being considered, including further optimization of the algorithm parameters and investigation of their influence on registration results. For example, the influence of the number of neighbors considered for bandwidths calculations during AMS clustering on the clusters' uniformity (i.e., the resemblance of the fibers within the cluster) should be investigated. As the number of considered neighbors increases, data may be over-smoothed and poor within-cluster uniformity occurs. This may interfere with the registration process since the basic assumption that the modes are reliable representatives of their fiber population is violated. Conversely, considering too few neighbors may lead to a large number of very small clusters resulting in an unnecessarily high computational load during registration. Alternative cost functions are being considered, including the use of the Kullback-Leibler distance for the GMMs registration phase. Other related issues include optimizing the initialization method for the GMMs registration and investigating its domain of convergence. Future work includes additional validation using more intra-subject data and finally, the extension to inter-

subject registration and non-linear registration.

V. APPENDIX

We examine invariance properties of the mean-shift algorithm under various spatial transformations, including pure translational transformation, pure rotational transformation and uniform (isotropic) scaling transformations. In the following, \mathbf{x} and \mathbf{y} are two 3P-dimensional fiber sets.

1) Pure translational transformation

Formally,

$$\mathbf{y} = \mathbf{x} + t \quad (21)$$

t is a translation vector.

Note that the kernel bandwidth h_i does not change under pure translational transformation:

$$h_i^t = \|y - y_{i,k}\| = \|x + t - (x_{i,k} + t)\| = \|x - x_{i,k}\| = h_i \quad (22)$$

The mean-shift algorithm is initialized from every sample point in the feature space. As such, it is guaranteed that for each point x_0 , a point y_0 exists such that

$$y_0 = x_0 + t \quad (23)$$

Substituting equation (21) in equation (7) we get:

$$\begin{aligned} y_{j+1} &= \frac{\sum_{i=1}^n \frac{1}{h_i^{d+2}} y_i g(\|\frac{y_j - y_i}{h_i}\|^2)}{\sum_{i=1}^n \frac{1}{h_i^{d+2}} g(\|\frac{y_j - y_i}{h_i}\|^2)} = \\ &= \frac{\sum_{i=1}^n \frac{1}{h_i^{d+2}} (x_i + t) g(\|\frac{x_j + t - (x_i + t)}{h_i}\|^2)}{\sum_{i=1}^n \frac{1}{h_i^{d+2}} g(\|\frac{x_j + t - (x_i + t)}{h_i}\|^2)} = \\ &= \frac{\sum_{i=1}^n \frac{1}{h_i^{d+2}} (x_i + t) g(\|\frac{x_j - x_i}{h_i}\|^2)}{\sum_{i=1}^n \frac{1}{h_i^{d+2}} g(\|\frac{x_j - x_i}{h_i}\|^2)} = \\ &= \frac{\sum_{i=1}^n \frac{1}{h_i^{d+2}} x_i g(\|\frac{x_j - x_i}{h_i}\|^2)}{\sum_{i=1}^n \frac{1}{h_i^{d+2}} g(\|\frac{x_j - x_i}{h_i}\|^2)} + t = x_{j+1} + t \end{aligned} \quad (24)$$

This property implies that the corresponding modes m_x and m_y also maintain the same spatial transformation i.e., $m_y = m_x + t$.

2) Pure rotational transformation

Formally,

$$\mathbf{y} = R\mathbf{x} \quad (25)$$

R is a rotation matrix. Since the rotation matrix R represents a linear transformation:

$$\begin{aligned} aR(x) &= R(ax) \\ R(\Sigma X_i) &= \Sigma R X_i \end{aligned} \quad (26)$$

where a is a scalar constant. Moreover, since the rotation matrix R is orthogonal, it is norm preserving i.e.,

$$\|R\mathbf{x}\| = \|\mathbf{x}\|. \quad (27)$$

Using equation (27) we show that the kernel bandwidths do not change under this transformation

$$h_i^t = \|y - y_{i,k}\| = \|R\mathbf{x} - R\mathbf{x}_i\| = \|R(\mathbf{x} - \mathbf{x}_{i,k})\| = \|\mathbf{x} - \mathbf{x}_{i,k}\| = h_i \quad (28)$$

Note that since rotation does not alter relative positions between sample points in the feature space, the following equality holds:

$$y_i^k = R x_i^k. \quad (29)$$

Substituting equation (25) in equation (7) and using the linearity of R we get:

$$\begin{aligned} y_{j+1} &= \frac{\sum_{i=1}^n \frac{1}{h_i^{d+2}} y_i g(\|\frac{y_j - y_i}{h_i}\|^2)}{\sum_{i=1}^n \frac{1}{h_i^{d+2}} g(\|\frac{y_j - y_i}{h_i}\|^2)} = \\ &= \frac{\sum_{i=1}^n \frac{1}{h_i^{d+2}} R x_i g(\|\frac{R x_j - R x_i}{h_i}\|^2)}{\sum_{i=1}^n \frac{1}{h_i^{d+2}} g(\|\frac{R x_j - R x_i}{h_i}\|^2)} = \\ &= \frac{\sum_{i=1}^n \frac{1}{h_i^{d+2}} R x_i g(\|\frac{R(x_j - x_i)}{h_i}\|^2)}{\sum_{i=1}^n \frac{1}{h_i^{d+2}} g(\|\frac{R(x_j - x_i)}{h_i}\|^2)} = \\ &= \frac{\sum_{i=1}^n \frac{1}{h_i^{d+2}} R x_i g(\|\frac{x_j - x_i}{h_i}\|^2)}{\sum_{i=1}^n \frac{1}{h_i^{d+2}} g(\|\frac{x_j - x_i}{h_i}\|^2)} = R x_{j+1} \end{aligned} \quad (30)$$

This property implies that the corresponding modes m_x and m_y also maintain the same spatial transformation i.e., $m_y = R m_x$.

3) Pure uniform (isotropic) scaling transformations

Formally,

$$\mathbf{y} = \alpha \mathbf{x} \quad (31)$$

where α is a uniform scaling factor. The kernel bandwidths change under this transformation:

$$h_i^t = \|y - y_{i,k}\| = \|\alpha x - \alpha x_i\| = \|\alpha(x - x_{i,k})\| = \alpha \|x - x_{i,k}\| = \alpha h_i, \quad (32)$$

Note that since isotropic scaling does not change relative positions between sample points in the feature space, the following equality holds:

$$y_i^k = \alpha x_i^k \quad (33)$$

Substituting equations (31) and (32) in equation (7), we get:

$$\begin{aligned} y_{j+1} &= \frac{\sum_{i=1}^n \frac{1}{(\alpha h_i)^{d+2}} \alpha x_i g(\|\frac{\alpha x_j - \alpha x_i}{\alpha h_i}\|^2)}{\sum_{i=1}^n \frac{1}{(\alpha h_i)^{d+2}} g(\|\frac{\alpha x_j - \alpha x_i}{\alpha h_i}\|^2)} = \\ &= \frac{\sum_{i=1}^n \frac{1}{\alpha^{d+2} h_i^{d+2}} \alpha x_i g(\|\frac{\alpha(x_j - x_i)}{\alpha h_i}\|^2)}{\sum_{i=1}^n \frac{1}{\alpha^{d+2} h_i^{d+2}} g(\|\frac{\alpha(x_j - x_i)}{\alpha h_i}\|^2)} = \\ &= \alpha \frac{\sum_{i=1}^n \frac{1}{h_i^{d+2}} x_i g(\|\frac{x_j - x_i}{h_i}\|^2)}{\sum_{i=1}^n \frac{1}{h_i^{d+2}} g(\|\frac{x_j - x_i}{h_i}\|^2)} = \alpha x_{j+1} \end{aligned} \quad (34)$$

This property implies that the corresponding modes m_x and m_y also maintain this spatial transformation i.e., $m_y = \alpha m_x$.

Acknowledgments:

This research was funded in part by a Strategic Research Directions grant from the Israeli ministry of sciences

REFERENCES

- [1] P. J. Basser, J. Mattiello, and D. Lebihan, "Mr diffusion tensor spectroscopy and imaging," *Biophysical Journal*, vol. 66, pp. 259–267, 1994.
- [2] P. J. Basser and C. Pierpaoli, "Microstructural and physiological features of tissues elucidated by quantitative-diffusion-tensor mri," *Journal of Magnetic Resonance*, vol. 111, no. 3, pp. 209–219, June 1996.
- [3] S. Mori, B. J. Crain, V. P. Chacko, and P. C. M. van Zijl, "Three dimensional tracking of axonal projections in the brain by magnetic resonance imaging," *Annals of Neurology*, vol. 45, pp. 265–269, 1999.
- [4] P. Basser, S. Pajevic, C. Pierpaoli, J. Duda, and A. Aldroubi, "In vivo fiber tractography using dt-mri data," *Magnetic Resonance in Medicine*, vol. 44, pp. 625–632, 2000.
- [5] M. Lazar, D. M. Weinstein, J. S. Tsuruda, K. M. Hasan, K. Arfanakis, M. E. Meyerand, B. Badie, H. A. Rowley, V. Haughton, A. Field, and A. L. Alexander, "White matter tractography using diffusion tensor deflection," *Human Brain Mapping*, vol. 18, pp. 306–321, 2003.
- [6] M. Bjornemo, A. Brun, R. Kikinis, and C. F. Westin, "Regularized stochastic white matter tractography using diffusion tensor mri," in *MICCAI '02: Proceedings of the 5th International Conference on Medical Image Computing and Computer-Assisted Intervention-Part I*. London, UK: Springer-Verlag, 2002, pp. 435–442.
- [7] P. Hagmann, J. Thiran, L. Jonasson, P. Vandergheynst, S. Clarke, P. Maeder, and R. Meuli, "DTI mapping of human brain connectivity: statistical fibre tracking and virtual dissection," *Neuroimage*, vol. 19, no. 3, pp. 545–554, 2003.
- [8] O. Friman, G. Farneback, and C. F. Westin, "A Bayesian approach for stochastic white matter tractography," *IEEE Transactions on Medical Imaging*, vol. 25, no. 8, pp. 965–978, 2006.
- [9] M. Lazar, P. Thottakara, A. Field, B. Laundre, B. Badie, B. Jellison, and A. Alexander, "A white matter tractography study of white matter reorganization after surgical resection of brain neoplasms," in *Proceedings of 12th ISMRM Scientific Meeting, Kyoto, Japan, 2004*, p. 1259.
- [10] S. H. Jang, S. H. Kim, S. H. Cho, B. Y. Choi, and Y. W. Cho, "Demonstration of motor recovery process in a patient with intracerebral hemorrhage," *NeuroRehabilitation*, vol. 22, no. 2, pp. 141–145, 2007.
- [11] I. Corouge, P. T. Fletcher, S. C. Joshi, J. H. Gilmore, and G. Gerig, "Fiber tract-oriented statistics for quantitative diffusion tensor mri analysis," in *Medical Image Computing and Computer-Assisted Intervention - MICCAI 2005, 8th International Conference, Palm Springs, CA, USA, October 26-29, 2005, Proceedings, Part I*, ser. Lecture Notes in Computer Science, J. S. Duncan and G. Gerig, Eds., vol. 3749. Springer, 2005, pp. 131–139.
- [12] L. J. O'Donnell and C. F. Westin, "Automatic tractography segmentation using a high-dimensional white matter atlas," *IEEE Transactions on Medical Imaging*, vol. 26, no. 11, pp. 1562–1575, 2007.
- [13] M. Maddah, W. Grimson, S. Warfield, and W. Wells, "A unified framework for clustering and quantitative analysis of white matter fiber tracts," *Medical Image Analysis*, vol. 12, no. 2, pp. 191–202, 2008.
- [14] D. Xu, S. Mori, D. Shen, P. C. van Zijl, and C. Davatzikos, "Spatial normalization of diffusion tensor fields," *Magnetic resonance in medicine*, vol. 50, pp. 175–182, 2003.
- [15] H. J. Park, M. Kubicki, M. E. Shenton, A. Guimond, R. W. McCarley, S. E. Maier, R. Kikinis, F. A. Jolesz, and W. C. F., "Spatial normalization of diffusion tensor MRI using multiple channels," *Neuroimage*, vol. 20, no. 4, pp. 1995–2009, 2003.
- [16] A. Leemans, J. Sijbers, S. De Backer, E. Vandervliet, and P. M. Parizel, "Affine coregistration of diffusion tensor magnetic resonance images using mutual information," in *Advanced Concepts for Intelligent Vision Systems, ACIVS, 2005*, pp. 523–530.
- [17] J. P. Thirion, "Image matching as a diffusion process: an analogy with maxwell's demons," *Medical Image Analysis*, vol. 2, pp. 243–260(18), September 1998.
- [18] A. Guimond, C. Guttman, S. Warfield, and C. F. Westin, "Deformable registration of dt-mri data based on transformation invariant tensor characteristics," *Biomedical Imaging, 2002. Proceedings. 2002 IEEE International Symposium on*, pp. 761–764, 2002.
- [19] J. Ruiz-Alzola, C. F. Westin, S. K. Warfield, C. Alberola, S. E. Maier, and R. Kikinis, "Nonrigid registration of 3d tensor medical data," *Medical Image Analysis*, vol. 6, no. 2, pp. 143–161, 2002.
- [20] G. K. Rohde, S. Pajevic, and C. Pierpaoli, "Multi-channel registration of diffusion tensor images using directional information," in *Proceedings of the 2004 IEEE International Symposium on Biomedical Imaging: From Nano to Macro ISBI, Arlington, VA, USA, 2004*. IEEE, 2004, pp. 712–715.

- [21] W. V. Hecke, A. Leemans, E. D'Agostino, S. D. Backer, E. Vandervliet, P. M. Parizel, and J. Sijbers, "Nonrigid coregistration of diffusion tensor images using a viscous fluid model and mutual information," *IEEE Trans. Med. Imaging*, vol. 26, no. 11, pp. 1598–1612, 2007.
- [22] H. Zhang, P. A. Yushkevich, D. C. Alexander, and J. C. Gee, "Deformable registration of diffusion tensor MR images with explicit orientation optimization," *Medical Image Analysis*, vol. 10, no. 5, pp. 764–785, 2006.
- [23] A. Goh and R. Vidal, "Algebraic methods for direct and feature based registration of diffusion tensor images," in *ECCV (3)*, 2006, pp. 514–525.
- [24] M. Pollari, T. Neuvonen, and J. Lötjönen, "Affine registration of diffusion tensor mr images," in *Medical Image Computing and Computer-Assisted Intervention MICCAI 2006*, ser. Lecture Notes in Computer Science, vol. 4191. Springer, 2006, pp. 629–636.
- [25] M. Pollari, T. Neuvonen, M. Lilja, and J. Lotjonen, "Comparative evaluation of voxel similarity measures for affine registration of diffusion tensor mr images," *Biomedical Imaging: From Nano to Macro, 2007. ISBI 2007. 4th IEEE International Symposium on*, pp. 768–771, April 2007.
- [26] A. Leemans, J. Sijbers, S. De Backer, E. Vandervliet, and P. Parizel, "Multiscale white matter fiber tract coregistration: a new feature-based approach to align diffusion tensor data," *Magnetic resonance in medicine*, vol. 55, pp. 1414–1423, 2006.
- [27] A. Mayer and H. Greenspan, "Direct registration of white matter tractographies and application to atlas construction," in *Workshop on Statistical Registration: Pair-wise and Group-wise Alignment and Atlas Formation*. Brisbane, Australia: MICCAI, November 2007.
- [28] U. Ziyang, M. R. Sabuncu, L. J. O'Donnell, and C. F. Westin, "Nonlinear registration of diffusion mr images based on fiber bundles," in *Tenth International Conference on Medical Image Computing and Computer-Assisted Intervention (MICCAI '07)*, ser. Lecture Notes in Computer Science, vol. 4791, Brisbane, Australia, November 2007, pp. 351–358.
- [29] O. Zvitia, A. Mayer, and H. Greenspan, "White matter tractographies registration using gaussian mixture modeling," in *Proceedings of the SPIE*, ser. Presented at the Society of Photo-Optical Instrumentation Engineers (SPIE) Conference, vol. 6914, no. 1. SPIE, April 2008, p. 69142G.
- [30] —, "Adaptive mean-shift registration of white matter tractographies," in *Proceedings of the 2008 IEEE International Symposium on Biomedical Imaging: From Nano to Macro, Paris, France, May 14-17, 2008*, May 2008, pp. 692–695.
- [31] B. Georgescu, I. Shimshoni, and P. Meer, "Mean shift based clustering in high dimensions: A texture classification example," in *ICCV '03: Proceedings of the Ninth IEEE International Conference on Computer Vision*, vol. 1. Washington, DC, USA: IEEE Computer Society, 2003, pp. 456–463.
- [32] D. Comaniciu and P. Meer, "Mean shift: a robust approach toward feature space analysis," *IEEE transactions on pattern analysis and machine intelligence*, vol. 24, no. 5, pp. 603–619, 2002.
- [33] D. Comaniciu, V. Ramesh, and P. Meer, "The variable bandwidth mean shift and data driven scale selection," in *Proc of ICCV/IEEE transactions on pattern analysis and machine intelligence*, vol. 1, 2001, pp. 438–445.
- [34] K. Fukunaga and L. D. Hostetler, "The estimation of the gradient of a density function, with applications in pattern recognition," *IEEE transactions on information theory*, vol. 31, pp. 32–40, 1975.
- [35] Y. Cheng, "Mean shift, mode seeking, and clustering," *IEEE transactions on pattern analysis and machine intelligence*, vol. 17, no. 8, pp. 790–799, 1995.
- [36] P. Indyk and R. Motwani, "Approximate nearest neighbors: towards removing the curse of dimensionality," in *STOC '98: Proceedings of the thirtieth annual ACM symposium on Theory of computing*. New York, NY, USA: ACM, 1998, pp. 604–613.
- [37] K. Okada, D. Comaniciu, and A. Krishnan, "Robust 3d segmentation of pulmonary nodules in multislice ct images," in *Medical Image Computing and Computer-Assisted Intervention MICCAI 2004*, ser. Lecture Notes in Computer Science, vol. 3217, 2004, pp. 881–889.
- [38] B. Jian and B. C. Vemuri, "A robust algorithm for point set registration using mixture of gaussians," *Computer Vision, 2005. ICCV 2005. Tenth IEEE International Conference on*, vol. 2, pp. 1246–1251, Oct. 2005.
- [39] M. Fischler and R. Bolles, "Random sample consensus: a paradigm for model fitting with application to image analysis and automated cartography," *Communication of the Assoc. Comp. Mach.*, vol. 24, pp. 381–395, 1981.
- [40] H. Jiang, P. C. M. van Zijl, J. Kim, G. D. Pearlson, and S. Mori, "Dstudio:resource program for diffusion tensor computing and fiber bundle tracking," *computer methods and programs in biomedicine*, vol. 81, no. 2, pp. 106–116, 2006.
- [41] M. Jenkinson and S. M. Smith, "A global optimisation method for robust affine registration of brain images," *Medical Image Analysis*, vol. 5, no. 2, pp. 143–156, 2001.
- [42] S. Smith, M. Jenkinson, M. Woolrich, C. Beckmann, T. Behrens, H. Johansen-Berg, P. Bannister, M. De Luca, I. Drobnjak, D. Flitney, R. Niazy, J. Saunders, J. Vickers, Y. Zhang, N. De Stefano, J. Brady, and P. Matthews, "Advances in functional and structural mr image analysis and implementation as fsl," *Neuroimage*, vol. 23, no. 1, pp. 208–219, 2004.
- [43] P. Besl and N. McKay, "A method for registration of 3-d shapes," *IEEE Transactions on Pattern Analysis and Machine Intelligence*, vol. 14, no. 2, pp. 239–256, 1992.